GDCh Research Article Angewandte International Edition Chemie www.angewandte.org

How to cite: *Angew. Chem. Int. Ed.* **2025**, *64*, e202418882
doi.org/10.1002/anie.202418882

Antibacterial Nanogels

pH-Responsive Polyglycerol Nanogels for Periodontitis Treatment through Antibacterial and Pro-Angiogenesis Action

Guoxin Ma, Ke Xu, Leixiao Yu, and Rainer Haag**

Abstract: Periodontitis is a microbe-driven inflammatory disease leading to bone resorption and tissue destruction. We propose a dual-functional nanogel complex armed with the antimicrobial drug triclosan (TCS) and the pro-angiogenesis medication deferoxamine (DFO) for combating microbial pathogens and promoting tissue regeneration. The nanogel system (NG-TCS-DFO) that we fabricated from linear polyglycerol exhibits well-defined spherical morphology and a positively charged surface for bacteria adhesion. The rapid and sustained degradation of NG-TCS-DFO in the acidic environment of an infection site induces the on-demand release of TCS and DFO. The NG-TCS-DFO shows potent bacteria elimination of the gingivitis-causing bacteria *Porphyromonas gingivalis* in both planktonic (99.9 %) and biofilm (99 %) states. Furthermore, the NG-TCS-DFO can promote vascularization and migration of human umbilical vein endothelial cells (HUVECs). Contributing to the synergistic effect of TCS and DFO, the NG-TCS-DFO demonstrates significant bone tissue regeneration and accelerated healing of periodontitis in vivo. This polyglycerol-based nanogel may therefore offer smart combined delivery of multiple therapeutics against bacteria-driven diseases.

Introduction

Periodontitis, one of the most prevalent chronic diseases among humans, is usually induced by bacterial infection and progresses rapidly from pocket formation to tissue resorption and eventually tooth loss.[1] The persistent inflammatory disorder caused by periodontitis may also be associated with various systemic diseases including cardiovascular diseases, diabetes mellitus and coronary syndrome.[2] The current state of the art for primary clinical treatment of periodontitis calls for non-surgical removal of tartar and plaque from the periodontal surface, followed by systemic antibiotics.[3] However, the dynamic nature of our oral environment, for instance the constant flow of saliva and the intense movement of ingestion, make it easy for bacteria colonies reestablish themselves in an inaccessible untreated area, then translocate to the newly treated area, leading eventually to the recurrence of periodontitis.[4] The key to curing periodontitis is to restore healthy gingival tissues to reduce the risk of bacterial infection and the level of inflammation.[5] This requires combination of antimicrobial agents and pro-angiogenesis medications in the post-debridement stage, but due to the drug molecules' poor biodistribution and insufficient in situ retention time,[6] a high dosage is often prescribed. This practice carries potential risks including prolonged treatment, activation of pro-inflammatory mediators and drug resistance.[7] Numerous local drug delivery systems (LDDS) have been developed to address these risks by regulating local drug concentration and minimizing adverse reactions.[6b,8] LDDS make new categories of drugs available for local periodontal therapy especially the water-insoluble drugs with poor adsorption e.g. Chlorhexidine.[9] Among the recently reported LDDS, nanoparticles are gaining extensive attention owing to their superb flexibility, targetability and biocompatibility.[10] Moreover, advanced nanoparticle design can achieve high loading capacity, precise targetability, responsiveness towards specific stimuli, controlled release kinetics, and so on.[11] Triclosan (TCS), a broad-spectrum antimicrobial agent, has been approved for incorporation in oral care products to prevent or reduce plaque formation.[12] However, TCS is a crystalline compound and poorly soluble in water. This severely limits not only the efficacy of TCS but also the scenarios where it can be applied. Deferoxamine (DFO) is a bacterial siderophore extracted from the medium of the *Streptomyces pilosus.* DFO has been repeatedly shown to promote angiogenesis by activating the expression of both vascular endothelial growth factor (VEGF)[13] and hypoxia inducible factor-1α (HIF-1α),[14] thereby facilitating tissue repair and wound healing.[15] More importantly, the vasculature plays a critical role in bone repair and functioning by delivering nutrients, minerals and osteogenic progenitors.[16] Although combined delivery of the antibiotics and pro-angiogenesis agents is a straightforward strategy to achieve satisfactory therapeutic efficacy and prevent recurrence, it is practically

[*] G. Ma, Prof. Dr. R. Haag
Institut für Chemie und Biochemie
Freie Universität Berlin
Takustr. 3, Berlin 14195, Germany
E-mail: haag@zedat.fu-berlin.de

K. Xu, Prof. Dr. L. Yu
State Key Laboratory of Oral Diseases, National Clinical Research Center for Oral Diseases
West China Hospital of Stomatology
Sichuan University
Chengdu 610064, China
E-mail: leixiaoyu@scu.edu.cn

challenging to devise a singular platform that is capable for loading of multiple agents varying physical and chemical properties, independently releasing them in a controlled manner and preserving their primary functions. Therefore, we synthesized linear polyglycerol functionalized with vinyl ether acrylate (VEA) and triethylammonium chloride (lPG-VEA-DEA) to fabricate the pH- responsive nanogel system that encapsulates both TCS and DFO (NG-TCS-DFO) for periodontitis treatment. As illustrated in the Scheme 1, the self-aggregation of the synthesized lPG-VEA-DEA occurs upon temperature increase, and the thermally pre-induced aggregates serve as precursors for the nanogel formulation. This strategy excludes the use of organic solvent and thus greatly improves the biosafety of the system. To minimize the off-site release of TCS, we modified the TCS with the VEA group, and the modified TCS can be jointly crosslinked with the nanogel then released in its original form via acetal cleavage under pH < 6. The therapeutic effects of NG-TCS-DFO are synergistically achieved through active binding to the bacteria and sustained release of the payloads. We investigated the size and the temperature dependence of the aggregates and further characterized the size, zeta potential, morphology, and degradation kinetics of the nanogel complex. We evaluated in vitro the antibacterial activities of NG-TCS-DFO against bacteria in both planktonic and biofilm growth stages. The pro-vascularization effect of NG-TCS-DFO was assessed in vitro by tube formation and migration of human umbilical vein endothelial cells (HUVECs). Lastly, we demonstrated in vivo that NG-TCS-DFO induces tissue regeneration and bone reconstruction. We therefore propose the new nanogel system, with its combined delivery of TCS and DFO, as a competent candidate for clinical translation against periodontitis.

Results and Discussion

Preparation and Characterization of Nanogel

Firstly, the block copolymer lPG-$AGE_{2.8\%}$ (Mw = 15 kDa) was synthesized via anionic polymerization as reported before.[17] Then we introduced the positive charge to the lPG-$AGE_{2.8\%}$ via thiol-ene click reaction between the allyl groups on the AGE block and the 2-diethylaminoethanethiol chloride. Subsequently, the obtained lPG-DEA was functionalized with the vinyl ether acrylate. Based on the previous study,[18] 10 % of the hydroxyl groups on the backbone of lPG were efficiently acetalized by the vinyl ether from VEA in the presence of catalytic amounts of pTSA. The DEA and VEA functionalities were determined by the ratio of integrals from the ^{1}H NMR spectra of lPG-VEA-DEA (Figure S1. DEA: δ 1.01 3H; VEA: δ 6.35 1H; lPG: δ 3.36–3.62 5H). The molecular weight of the obtained lPG-$DEA_{2.5\%}$-$VEA_{10\%}$ measured by GPC is 19.6 kDa (Figure S2). Then we employed the lPG-$DEA_{2.5\%}$-$VEA_{10\%}$ equipped with the acetal linker and acrylate crosslinker for nanogel formulation. Interestingly, we observed the low critical solution temperature (LCST) when the synthesized lPG-DEA-VEA is dissolved in water (Figure S3). The temperature-dependent aggregation measured by dynamic light scattering (DLS) (Figure 1B) indicates the polymer aggregates at the critical point of 19 °C. The presence of hydrophobic acrylates disrupts the intra and intermolecular hydrogen bonding among the water molecules and the -OH groups on the lPG backbone. Moreover, this is enhanced when the temperature increases up to 37 °C. Thus, we designed a solvent-free approach to construct the nanogel via the thermo-exchange procedure. Through the hydrophobic interactions, the photo initiator added to the aqueous solution of lPG-DEA-VEA can be

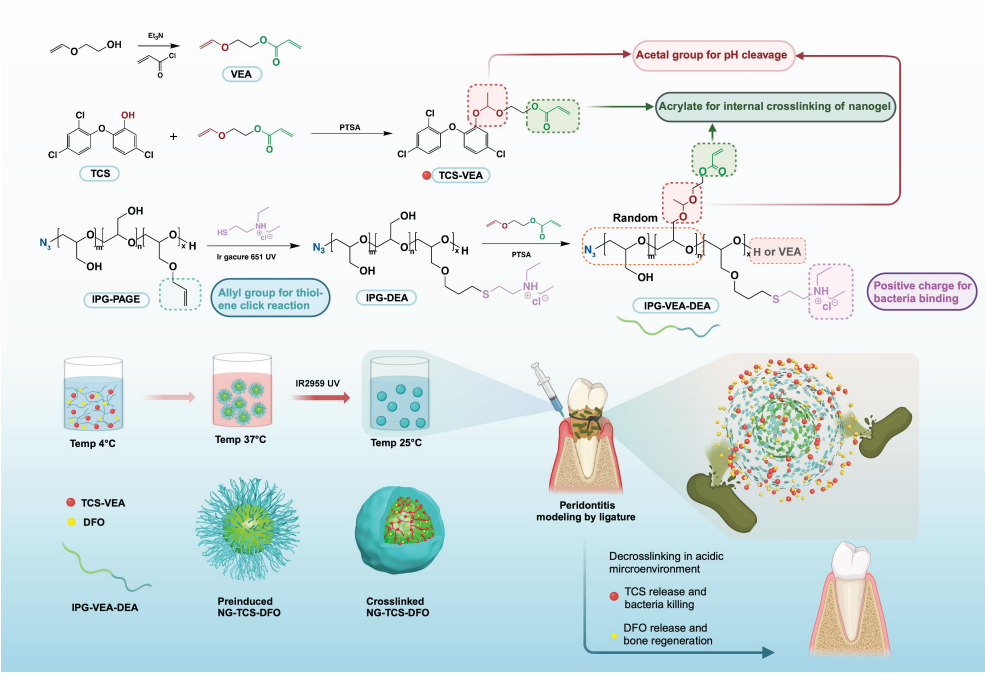

Scheme 1. Synthesis and formulation of the bifunctional nanogel complex (NG-TCS-DFO) for periodontitis treatment in vivo.

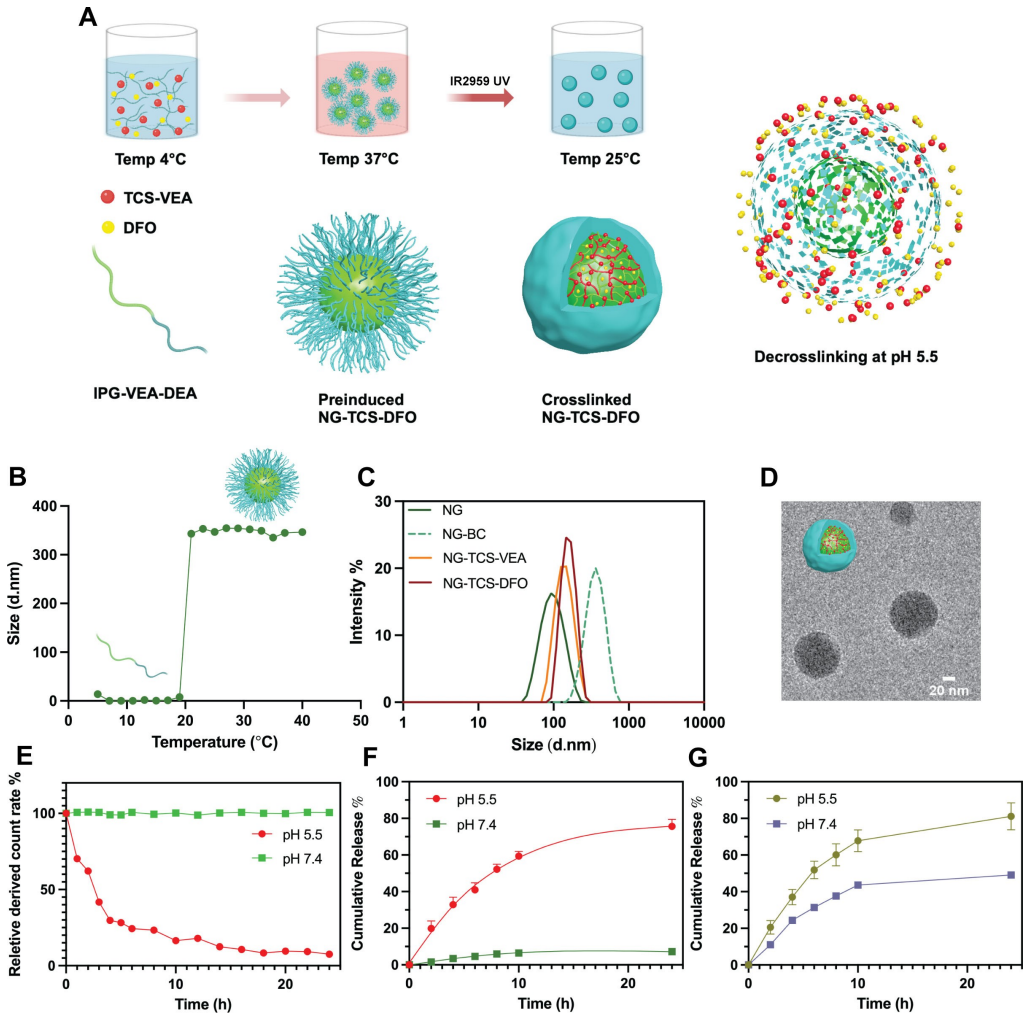

Figure 1. (A) Schematic illustration of nanogel fabrication. Characterization of the nanogels: NG-BC (before crosslinking), NG (after crosslinking), NG-TCS-VEA (after crosslinking and loading with TCS) and NG-TCS-DFO (after crosslinking and loading with TCS and DFO). (B) Temperature-dependent self-assembly behavior of NG-BC determined by DLS. (C) Size distribution measured by DLS. (D) Cryo-EM images of NG-TCS-DFO (scale bar: 20 nm). (E) Derived count rate of crosslinked NG particles measured by DLS varying pH value. In vitro release study of NG-TCS-DFO under pH 5.5 and pH 7.4: Triclosan (F) measured by HPLC and Deferoxamine (G) measured by plate reader at absorbance of 439 nm.

encapsulated into the aggregates induced by rising temperature. The acrylate groups on the hydrophobic VEA unites distributed internally are covalently crosslinked under the UV irradiation. To integrate multiple functions including reducing cytotoxicity, targeted on-site release, bacteria killing and enhancing tissue regeneration onto the nanogel complex, we intend to incorporate the nanogel with the antibacterial agent triclosan (TCS) and the deferoxamine (DFO) approved for enhancing tissue regeneration. Since the payloads are mainly loaded via physical interactions in the traditional drug carriers, and risks such as off-target leakage and depressed stability are frequently involved, we accordingly modified the triclosan with the VEA similarly as the lPG. The derived TCS-VEA exhibits the same acetal linker (δ 5.81 1H, -OC**H**OCH_3-) and the acrylate crosslinker (δ 6.35 1H, CH_2C**H**COO-) as the lPG-DEA-VEA (Figure S4), hence the TCS-VEA can be covalently encapsulated inside the nanogel while crosslinking. We characterized the nanogel before and after crosslinking by Fourier transform infrared spectroscopy (FT-IR), and it showed the stretch at 1625 cm^{-1} (C=C) remarkably weakened after crosslinking (Figure S5). The size and dispersity of pre-induced nanogel (NG-BC), the crosslinked nanogel (NG) and nanogel loaded with TCS-VEA and nanogel loaded with TCS-VEA and DFO were determined by DLS (Figure 1C). The average size of pre-induced nanogel is 460 nm and the size shrinks to 159 nm after crosslinking. The nanogel expands slightly to 177 nm after loaded with TCS-VEA and the nanogel loaded with the TCS-VEA and the DFO exhibits the average size of 181 nm. The crosslinked nanogel presents a well-defined spherical structure in the image (Figure 1D and Figure S6) taken by cryo electron microscopy (cryo-EM). In Figure S7, we further confirmed the crosslinked spherical structure of nanogels in air phase with atomic force microscopy (AFM). In addition, the zeta potential of 36.8 eV at pH 5.5 and 27.4 eV at pH 7.4 have verified the positively charged surface of the nanogel complex (Table 1). It is well established that the hydrolysis of the acetal linkers occurs rapidly in the acidic environment[19] and therefore, the nanogel fabricated from the

Table 1: Summary of size and loading efficiency of the bifunctional nanogels.

Copolymer	M_w (kDa)	Size (nm)[a]	Size (nm)[b]	Size (nm)[c]	PDI[c]	Zeta Potential [eV] [c]		DLC (wt. %)				DLE %	
						pH 5.5	pH 7.4	Theory		Determined		TCS	DFO
								TCS	DFO	TCS	DFO		
lPG-$DEA_{2.5\%}$-$VEA_{10\%}$	19.6	460	159	177	0.17	36.8	27.4	13	5	9.7	1.3	88.4	20.6

[a] pre-induced nanoaggregates. [b] crosslinked nanogel without payloads. [c] crosslinked nanogel with payloads.

lPG-DEA-VEA can be degraded into the lPG backbone with DEA units and acetaldehyde by pH stimuli. Consequently, the decrosslinking of the nanogel enforces the release of payloads on the targeted sites. Moreover, the acetal groups on the modified TCS-VEA can be correspondingly cleaved under the acidic conditions, which exclusively enables the TCS release in its original form. The size of the native lPG is around 5 nm[20] and thus the produced lPG and acetaldehyde can be readily eliminated by the renal clearance. The derived count rate as a representative of the number of particles in the nanogel suspension is investigated by DLS (Figure 1E). The number of particles in the nanogel solution decreases immediately after incubated with the PBS buffer at pH 5.5. More than half of the nanogel particles collapse after 3 hours and the number of particles remains consistent after 10 hours. The size change of nanogels under acidic environment was characterized by DLS (Figure S8). After 2-hour incubation in acetate buffer (pH = 5.5), the nanogels tended to swell rapidly due to acetal cleavage. Meantime we observed that small particles around 10 nm appeared. After 24 hours, the size of all particles decreased below 10 nm. In contrast, we observed no significant size change when the nanogels were placed in PBS buffer (pH = 7.4). For the encapsulated nanogel, the drug loading efficiency (DLE%) of TCS-VEA and DFO is 88.4 % and 20.6 %, respectively. The rather high DLE% of TCS-VEA is achieved by the covalent loading during the co-crosslinking. To mimic the slightly acidic microenvironment of the periodontitis with *Porphyromonas gingivalis* (*P. gingivalis*) infection, the release study of the NG-TCS-DFO is carried out in neutral and acidic buffer, and the release kinetics are shown in Figure 1F (TCS) and Figure 1G (DFO). Approximately 60 % of the TCS is released from the nanogel treated by acidic buffer in a controlled manner in the first 10 hours and the total amounts of 78 % of the TCS is released from the nanogel after 24 hours. Strikingly, the NG-TCS-DFO incubated in the neutral medium exhibits negligible leakage of the TCS (~6%) due to the co-crosslinking strategy. Moreover, we confirmed the TCS is released in the original form instead of VEA-modified version by the retention time in HPLC (Figure S9). On the other hand, the cumulative content of the released DFO is around 72 % after 24 hours, while the rate of release is faster compared to TCS. Moreover, over 50 % the DFO is retained without pH stimuli after 24 hours. It is evident that the joint chemical and physical interactions of the NG-TCS-DFO can sufficiently reduce the leakage in circulation and ensure the local release.

In-Vitro Anti-bacteria Activity Study of the Nanogel Complex

Periodontitis is frequently associated with localized chronic bacterial infection, and *P. gingivalis* is recognized as a representative periodontal pathogen.[21] We therefore set out to measure the anti-bacteria efficacy of the NG-TCS-DFO complex in vitro against *P. gingivalis.* We began by incubating the TCS-VEA, NG and NG-TCS-DFO in planktonic bacteria culture. Then we evaluated the bactericidal activity by plate counting. As shown in the Figure 2A, the number of colonies is significantly lower after treatment with NG-TCS-DFO, while the plates of TCS-VEA and unloaded nanogels display only moderate loss of colonies as compared to the control group. We then quantified the colony forming units and bacteria ratio of each group after treatment, as indicated in Figure 2B. Interestingly, VEA modification has greatly weakened the antimicrobial effect of triclosan: while native triclosan exhibits a minimal bactericidal concentration of 0.1–8 μg/mL,[22] we found that approximately 8.8 % of bacteria remained active after incubation with TCS-VEA at the concentration of 50 μg/mL. We also found that unloaded nanogels eliminated about 35 % of bacteria. The nanogel's positively charged shell can actively attach to the phosphate, carboxyl and saccharide groups on the surface of *P. gingivalis*, disrupting its cell membrane and inhibiting of the adhered bacteria. Strikingly, a 99.9 % bactericidal ratio was achieved by NG-TCS-DFO at a concentration of 50 μg/mL containing 0.48 μg/mL of TCS-VEA. This result makes clear that the triclosan was released in its original form due to the acetal cleavage and degradation of the nanogels in acidic environment. Furthermore, the bactericidal activity of the NG-TCS-DFO was remarkably enhanced by the positive charges on the nanogel surface, which pursues locating of the planktonic bacteria by electrostatic attraction. We continued our investigation of bactericidal efficacy through fluorescence microscopy after live/dead staining (Figure 2C). The corresponding live/dead bacteria ratio is quantified by the fluorescence intensity of each group (Figure 2D). The bacteria treated by the NG-TCS-DFO presented the strongest fluorescence from the dead cells, followed by those treated with TCS-VEA and the blank nanogel, which aligns with the previous results obtained via the plate counting assay.

Due to incomplete sanitation, oral plaques are frequently formed in the existent dental cavities. High consumption of glucose and lactose causes continuous biofilm accumulation and production of extracellular polymeric substances (EPS) which attributes to resist immune stress.[1a,23] Moreover, the low pH induced by the biofilm formation tends to promote the generation of EPS, and vice

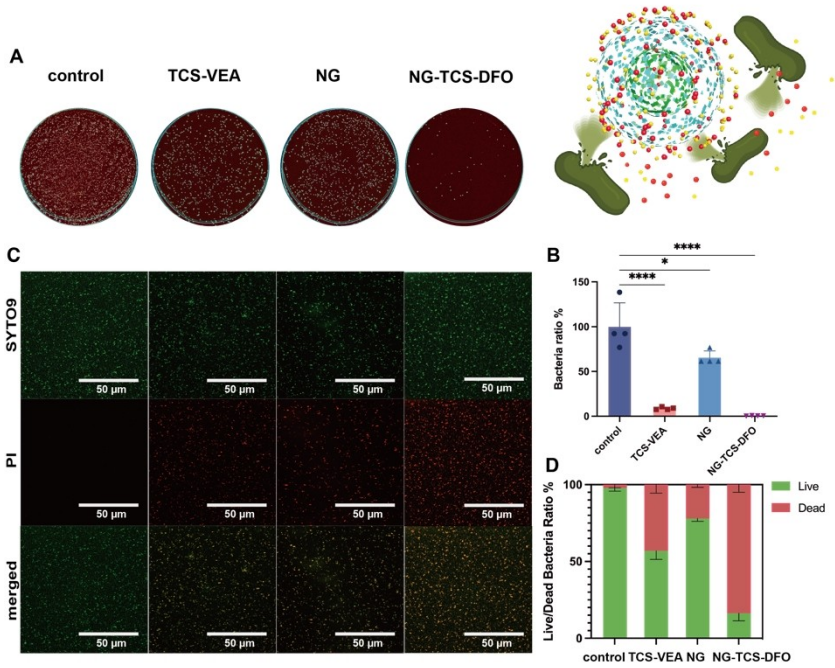

Figure 2. (A) Colonies of *Porphyromonas gingivalis (P. gingivalis)* on blood agar plate after treatment by TCS-VEA, NG or NG-TCS-DFO. Images were processed by Image J, using edge detection. (B) Antibacterial ratio of TCS-VEA, NG and NG-TCS-DFO (*$p = 0.011$, ****$p < 0.0001$). (C) Fluorescence microscopy images of *P. gingivalis* (live/dead stained using SYTO 9 and propidium iodide) after treatment with TCS-VEA, NG or NG-TCS-DFO for 24 h (scale bar: 50 μm). (D) Statistical study of live/dead bacteria by fluorescent intensity after treatment (5 images from same group were processed with Image J).

versa. The rapid propagation of the dental biofilm can ultimately cause the loss of supporting tissues, resorption of alveolar bones, and systemic periodontal issues.[24] We therefore investigated the anti-biofilm efficacy of the nanogel system. Firstly, we evaluated the mass of biofilm after treatment with TCS-VEA, blank nanogel, and nanogel loaded with triclosan and deferoxamine via the crystal violet assay (Figure 3A and 3B). The biofilm treated with unloaded nanogels and TCS-VEA lost 53 % and 67 % of their mass, respectively, while the biofilm incubated with NG-TCS-DFO showed shrinkage up to 85 %. The biofilm treated by NG-TCS-DFO also showed the least content stained in purple. Furthermore, we cultured the treated biofilms on blood agar plates, then obtained the surviving bacteria ratio via colony counting. As shown in Figure 3C, the unloaded nanogels and the TCS-VEA respectively inhibited nearly 54 % and 67 % of the bacteria from the biofilm, which is highly consistent with the mass loss. By comparison, NG-TCS-DFO achieved an exceptional anti-biofilm bactericidal rate of 99 %. Interestingly, we observed that the bactericidal efficacy of the TCS-VEA decreased significantly from 91 % to 46 %, when applied to the biofilm instead of planktonic bacteria, while the unloaded nanogel performed similarly in both circumstances. We suggest the reduced efficacy of the free therapeutics was caused by poor penetration through the EPS structure. The positively charged nanogel complex NG-TCS-DFO can bind bacteria and precisely proceed killing by constant release of triclosan, which disrupts the aggregation of biofilm. Meanwhile, we verified the of biofilms' architecture via 3D confocal laser scanning microscopy (Figure 3A). Overall, the number of dead cells increases from the blank nanogels, TCS-VEA to NG-TCS-DFO, whereas the biofilm after NG-TCS-DFO culture exhibits particularly high density of dead cells. This evidences the NG-TCS-DFO combats against bacteria coordinatively with effective penetration and on-site drug release. We further characterized the morphology of the bacteria after treatment using scanning electron microscopy. As seen in Figure 3A, membrane lysis and destruction occurred on most bacteria after treatment with NG-TCS-DFO, while the bacteria in the biofilms cultured with the NG or TCS-VEA were only partially damaged and distorted. These comprehensive in vitro studies soundly demonstrate the robust anti-bacteria and anti-biofilm properties of NG-TCS-DFO, and we therefore assume that the NG-TCS-DFO may function adequately in vivo as well.

In-Vitro Evaluation of Tube Formation and Migration of HUVECs Induced by Nanogel System

Since the clinical application requires excellent biocompatibility, we assessed the cytotoxicity of the nanogel series (50 μg /mL) using human gingival fibroblasts (HGF). Basically, the HGF were incubated for 24 hours to 72 hours with either the nanogel, the nanogel loaded with triclosan or the nanogel loaded with triclosan and deferoxamine. The cell viability for each group was quantified by CCK8 assay.

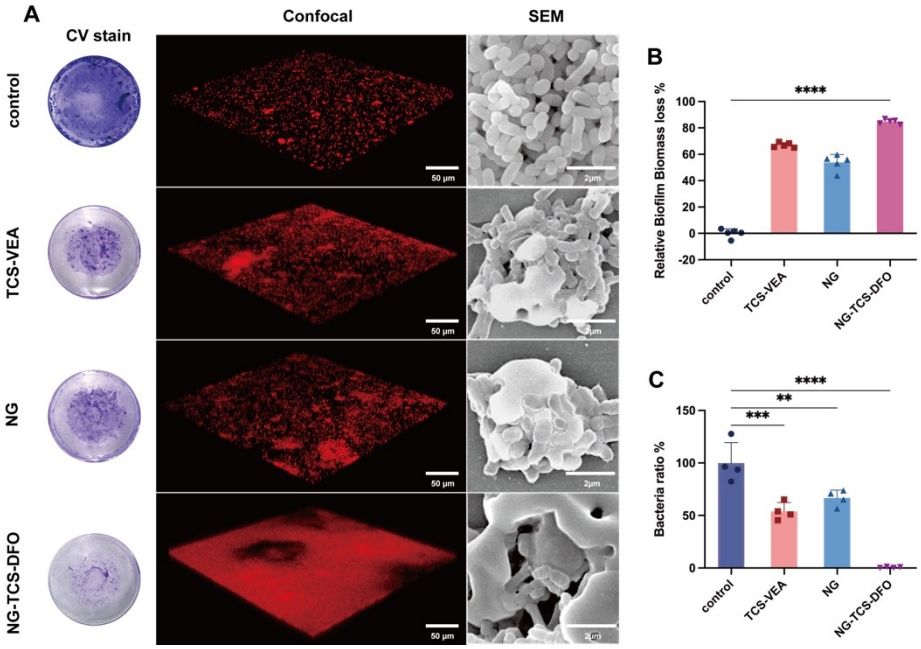

Figure 3. (A) Antibiofilm profile of TCS-VEA, NG or NG-TCS-DFO. Left: Biofilm stained by crystal violet. Middle: confocal laser scanning images of dead cells on biofilm stained by propidium iodide (scale bar: 50 μm). Right: scanning electric microscopy images of biofilm treated by overnight (scale bar: 2 μm). (B) Biomass loss of biofilm after treatment by TCS-VEA, NG or NG-TCS-DFO overnight using crystal violet assay (****$p < 0.0001$). (C) Bacteria ratio from biofilm incubated with TCS-VEA, NG or NG-TCS-DFO (**$p = 0.0033$, ***$p = 0.0003$, ****$p < 0.0001$).

In addition, the cytotoxicity of DFO was prescreened on the human umbilical vein endothelial cells (HUVECs) (Figure S10). The optimal concentration of DFO was determined to be 10 μg /mL based on its efficiency in promoting tissue regeneration and its potential toxicity at high doses. As is shown in Figure S11, the cell viability of HGF from all the groups was above 95 %, with no apparent difference as compared to the control group. We also investigated the morphology of HGF after incubation with NG, NG-TCS-VEA and NG-TCS-DFO, using nucleolus and cytoskeleton staining. The HGF from all groups presented intact structure with centrally located oval nucleus and elongated framework. These results confirm the safety of the NG-TCS-DFO at its working concentration. The reconstruction of the vascular network within bone defects is a primary prerequisite for bone regeneration. Plenty of studies have revealed that the deferoxamine can enhance the expression of hypoxia-inducible factor-1α (HIF-1α) and vascular endothelial growth factor (VEGF), both of which are associated with cell metabolism, proliferation and angiogenesis.[25] Here we performed vascularization of the HUVECs on Matrigel and visualized the tube formation induced by the NG, NG-TCS-VEA and NG-TCS-DFO using bright-field microscopy. The HUVECs induced by the NG-TCS-DFO tend to aggerate, with junctures extending to form a network (Figure 4A). We also counted and analyzed the number of meshes and junctions as well as the total length of tubes in each group; the results are shown in Figure 4B, 4C and 4D, respectively. In the HUVECs incubated with NG-TCS-DFO, the number of meshes was nearly tripled as compared to the control group, and the number of junctions increases up to 1.5-fold. These HUVECs treated by NG-TCS-DFO also showed an increase around 20 % in total tubule length, while we observed no significant enhancement among rest of the groups. In addition, we analyzed the expression of HIF-1α and VEGF in HUVECs after the various treatment. The NG-TCS-DFO group significantly upregulated the gene expression of both HIF-1α (Figure 4E) and VEGF (Figure 4F) on HUVECs, while no significant effect was observed in other groups. These results confirm that NG-TCS-DFO promotes angiogenesis by releasing DFO. To mimic the tissue regeneration process in vivo, we further investigated the ability of NG-TCS-DFO to stimulate the migration of HUVECs (Figure 4G). After 24 hours, the HUVECs treated by unloaded nanogel and NG-TCS-VEA exhibited moderate migration activity: 51 % of the scratched area is closed, which is close to the value seen with the control group. NG-TCS-DFO performed much better: in its presence, the area of the scratch reduced by up to 63 % (Figure 4H). Moreover, we determined the cell viability of HUVECs under the conditions mentioned above (Figure 4I) and all the groups presented superb biocompatibility.

In-Vivo Assessment of Nanogel Complex for Periodontitis Treatment

Based on the promising results in vitro, we further explored the therapeutic potential of the nanogel complex on the C57BL/6 mice with chronic periodontitis. We established the chronic periodontitis model through one-week ligation around the maxillary second molar, and we then treated the mice with

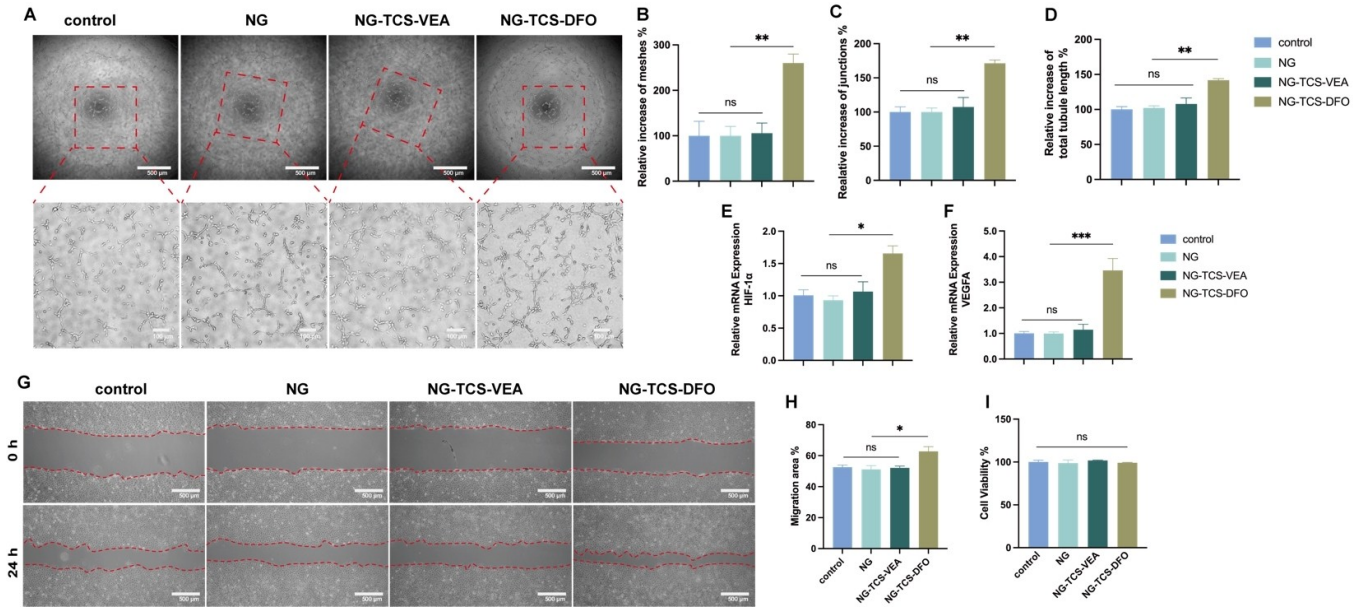

Figure 4. (A) Images of tubes formed from human umbilical vein endothelial cells (HUVECs) after 4 h incubation with NG, NG-TCS-VEA or NG-TCS-DFO (top scale bar: 500 μm; bottom scale bar: 100 μm). Quantitative analysis of the tube formation assay of HUVECs: (B) relative increase of meshes % (ns > 0.9999, **p = 0.0068). (C) Relative number of junctions % (ns > 0.9999, **p = 0.0019) and (D) relative total tubule length % (ns > 0.9999, **p = 0.0025). (E). qRT-PCR analysis of HIF-1α expression in HUVECs after treatment (ns > 0.9999, *p = 0.0158). (F). qRT-PCR analysis of VEGF expression in HUVECs after treatment (ns > 0.9999, ***p = 0.0009). (G) Images of the migration experiment of HUVECs (scale bar: 500 μm). (H) Statistical study of scratched area after 24 h treatment of NG, NG-TCS-VEA or NG-TCS-DFO (ns > 0.9999, *p = 0.0208). (I) Cell cytotoxicity evaluation of HUVECs after incubation with NG, NG-TCS-VEA or NG-TCS-DFO for 24 h (ns > 0.9999).

NG-TCS-VEA and NG-TCS-DFO for 2 weeks. Afterwards we verified the ligation-induced periodontitis and evaluated bone defect repair level by micro computed scanning tomography (micro-CT) of the alveolar bones. As shown in Figure 5A, we observed severe bone loss and gingival tissue recession in the ligated group. After 2-week treatment with NG-TCS-VEA or NG-TCS-DFO, we can clearly see the reduced bone resorption indicated in yellow (Figure 5B). Furthermore, we measured the linear distance between the cement enamel junction and the alveolar bone crest (CEJ-ABC) from the micro-CT images and compared this value among different groups (Figure 5C). The CEJ-ABC distance in mice with periodontitis was approximately 322 μm, while it fell to 230 μm and 206 μm after treatment with NG-TCS-VEA and NG-TCS-DFO, respectively. The bacteria aggregation definitively accelerates the progression of periodontitis, and vice versa. These results demonstrates that NG-TCS-VEA has greatly suppressed the aggravation of periodontitis by its superior bactericidal efficiency, and that it may have assisted the regeneration of periodontal tissues and alveolar bone. They also show that the dual-function NG-TCS-DFO, equipped with both anti-bacterial reagent TCS and bone repair booster DFO, can achieve integral therapy. In the post-bactericidal stage, the NG-TCS-DFO can greatly promote the tissue regeneration by the in situ release of DFO, which induces primary angiogenesis. Moreover, we quantified the bone mineral density (BMD) and the bone volume per tissue volume (BV/TV%) (Figure 5D, 5E). As expected, the NG-TCS-DFO-treated group exhibited the highest BMD of 460 mg HA/ccm and BV/TV% of 39.4 %, followed by the NG-TCS-VEA-treated group, with BMD of 399 mg HA/ccm and BV/TV% of 32.5 %. However, the ligated group treated with saline shows significantly lower BMD and BV/TV%, which are 323.1 mg HA/ccm and 24.3 %. These consistent results demonstrate the exceptional efficacy of NG-TCS-DFO against periodontitis. We then performed hematoxylin and eosin staining (H&E staining) of the collected specimen to investigate the periodontium status (Figure 5F). Again, we noticed the distinguished gingival atrophy and bone loss in the ligated group, and mild tissue regeneration in the NG-TCS-VEA treated mice. Surprisingly, the papillary connective tissues of the group treated by NG-TCS-DFO exhibited rather similar volume as compared to the healthy mice. These results show the extraordinary efficiency of NG-TCS-DFO in periodontitis treatment, owing to its multi-therapeutic encapsulation and rapid stimuli-responsive drug release. We further evaluated the biosafety of the nanogel series by H&E staining of the main organs including heart, liver, spleen, kidney, and lung. No pathological damage was caused by the two-week treatment with NG-TCS-VEA or NG-TCS-DFO (Figure S12).

We further performed Masson's trichrome staining of the decalcified bone to investigate the distribution of newly formed bones and surrounding tissues. As shown in Figure 6A, we observed hardly any freshly generated bone structure in the ligated group, seeing instead severe collagen loss and fiber discontinuity. In contrast, the NG-TCS-VEA and NG-TCS-DFO groups showed both newly formed bone and soft tissue structure. Though the newly formed tissue of NG-TCS-VEA group exhibited higher collagen density, the discontinuous arrangement was more significant. While the NG-TCS-DFO

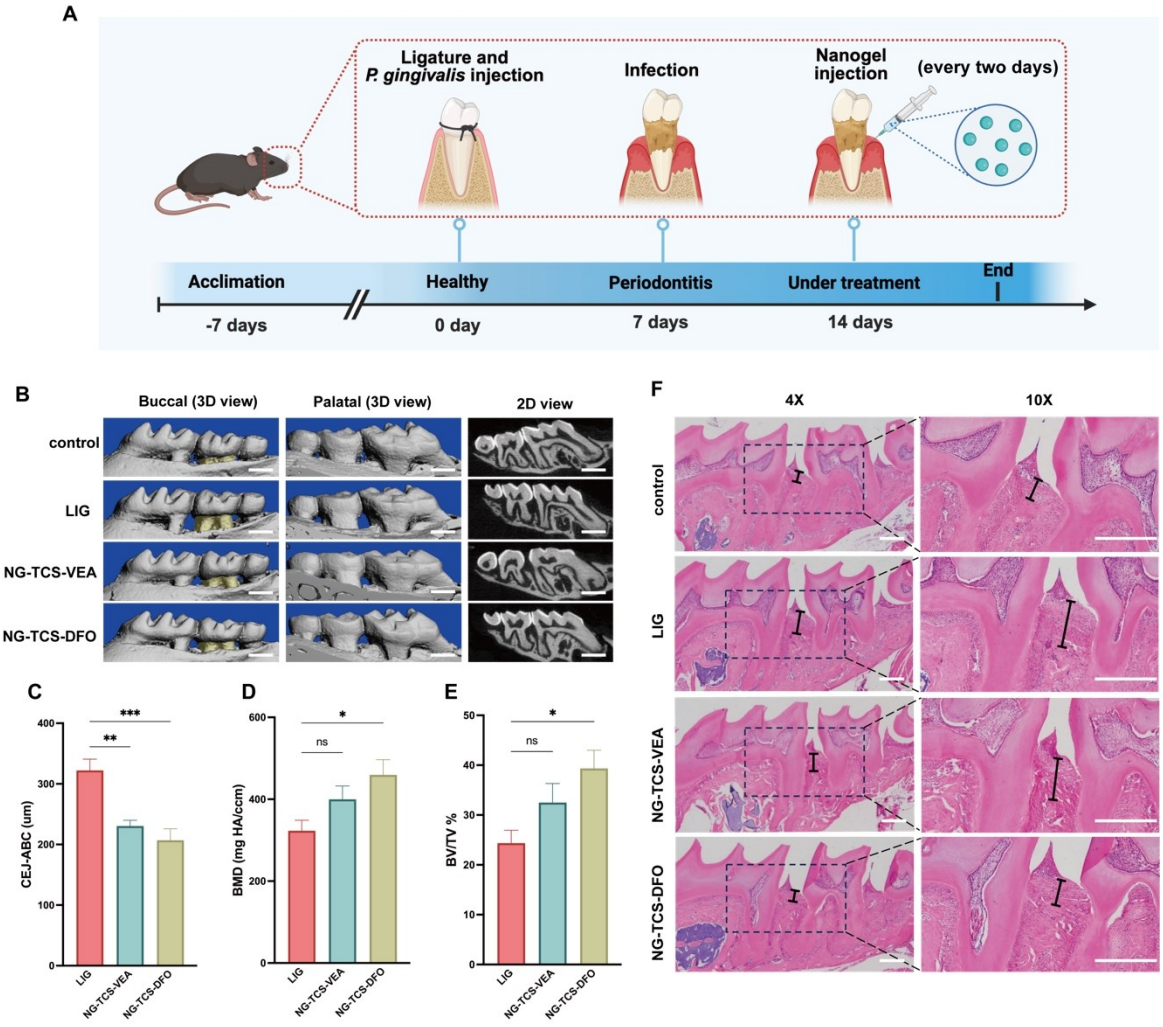

Figure 5. (A) Schematic illustration of treatment process in vivo. (B) Micro-CT evaluation of alveolar bone in healthy mice and *P. gingivalis* infected mice treated with saline, NG-TCS-VEA or NG-TCS-DFO (scale bar: 1 mm). Quantitative micro-CT analysis of alveolar bone with experimental periodontitis after treatment with saline, NG-TCS-VEA or NG-TCS-DFO: (C) CEJ-ABC (distance from cement enamel junction to alveolar bone crest; $^{**}p = 0.0024$, $^{***}p = 0.0003$), (D) BMD (bone mineral density; ns > 0.9999, $^{*}p = 0.0129$) and (E) BV/TV (%) (bone volume/tissue volume; ns > 0.9999, $^{*}p = 0.0163$). (F) H&E staining of alveolar bone in healthy mice, *P. gingivalis* infected mice treated with saline, NG-TCS-VEA or NG-TCS-DFO (scale bar: 200 μm).

group presented a more advanced stage of healing, the newly generated fibrous tissue was compacted and homogeneously distributed allowing the connective tissue with high collagen content to sufficiently support the corresponding alveolar bone. CD31-positive vascular cells are crucial for intercellular junction development and capillary formation especially during inflammation.[26] Therefore, we assessed the vascularization activity through sectional immunohistological staining with CD31 antibody. As shown in Figure 6B, the amounts of newly formed blood vessels were slightly higher in the NG-TCS-VEA group in comparison with the ligated group, while the NG-TCS-DFO group presented the strongest intensity of CD31 indicating the highest number of newly formed blood vessels. Besides, the NG-TCS-DFO group also exhibited well-defined elongated tubular structure and elliptical rings, suggesting the accelerated healing process regulated by the cooperation of TCS and DFO. We also quantified the ratio of CD31-positive cells by statistical analysis of the stained area (Figure 6D). After treatment with NG-TCS-DFO, the amount of CD31 was nearly doubled as compared to the control. Furthermore, we used the Simple Ultrafast Multicolor Immunolabelling and Clearing (SUMIC) approach for the whole-tissue mapping of vessels, with results demonstrating outstanding tube formation in the NG-TCS-DFO group (Figure S13). We also used Immunohistochemical (IHC) staining to characterize ALP and IL-6 expression using, which are respectively associated with osteoblast differentiation[27] and inflammatory diseases and malignancies.[28] We can clearly see a distinctly higher intensity of ALP marker in the NG-TCS-DFO group in contrast to any other group (Figure 6C): the density of stained ALP is 862 % stronger than in the ligated group; the corresponding value for NG-TCS-VEA is 385.8 % (Figure 6E). The amplified ALP activity of NG-TCS-VEA and NG-TCS-DFO demonstrates that the elimination of bacteria

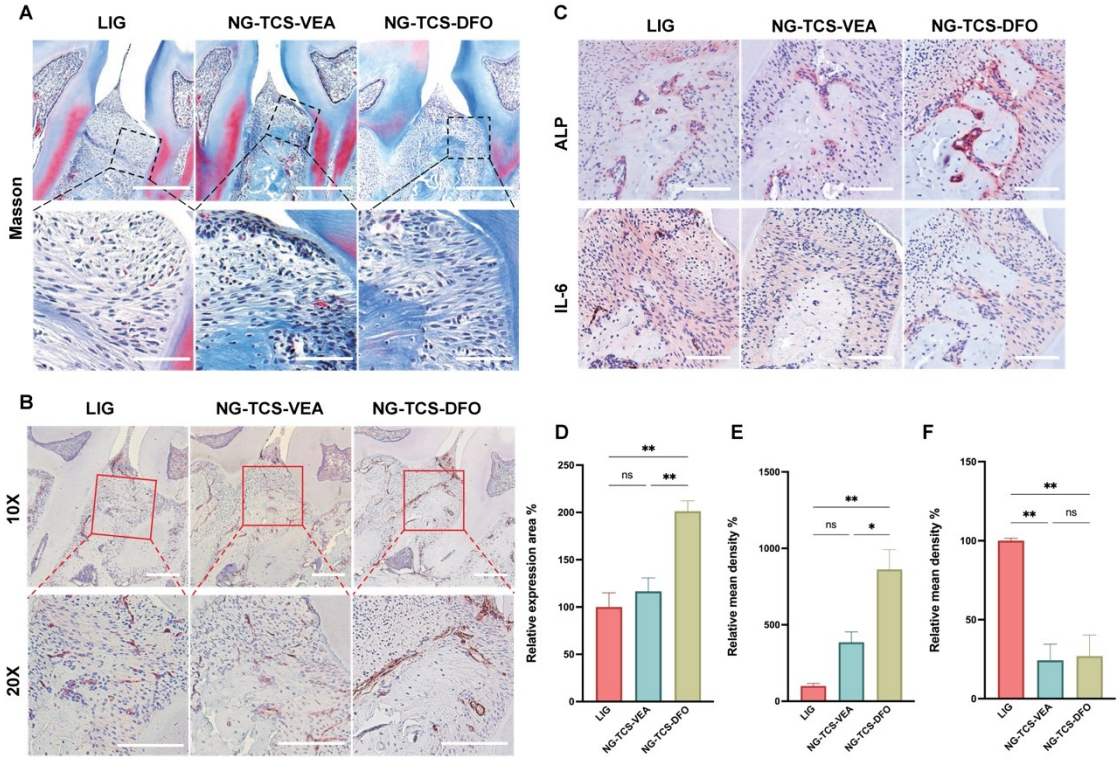

Figure 6. (A) Masson's trichrome stained ligated periodontal tissue after treatment by NG-TCS-VEA or NG-TCS-DFO (Top scale bar: 200 μm. Bottom scale bar: 50 μm). (B) Immunohistochemical staining of CD31 in bone vascularization (scale bar: 50 μm) and (D) corresponding analysis of CD31 expression (ns = 0.6764, **p = 0.0013, **p = 0.0043). (C) ALP and IL-6 stained periodontal tissues after treated by NG-TCS-VEA or NG-TCS-DFO (scale bar: 100 μm). Quantification analysis of staining intensity of ALP (E) (ns = 0.6221, **p = 0.0021, *p = 0.0174) and IL-6 (F) (ns = 0.9794, **p = 0.037, **p = 0.0044).

and the stimulation of angiogenesis by DFO synergistically enhance the osteogenesis. In the IHC staining of IL-6 (Figure 6F), the ligated group manifested a great number of IL-6 positive cells, indicating the local inflammation. By contrast, we observed notably weakened signals of IL-6 in the NG-TCS-VEA-treated and NG-TCS-DFO-treated groups. According to the statistical study of the mean intensity, the respective IL-6 intensity is relatively reduced to 26.93 % and 24.25 % after treatment with NG-TCS-VEA and NG-TCS-DFO, respectively. We attribute these anti-inflammatory effects primarily to the bactericidal activities of TCS.

Conclusion

We developed pH-responsive nanogels loaded with triclosan and deferoxamine to address long-standing challenges in periodontitis treatment. The resulting nanogel complex, NG-TCS-DFO, demonstrated superior loading efficiency and sustained stimuli-responsive release. The integrated encapsulation of both TCS and DFO bestows the dual functions of NG-TCS-DFO: killing bacteria and promoting angiogenesis. The NG-TCS-DFO shows exceptional efficiency against both planktonic bacteria and biofilm. We also verified in vitro that NG-TCS-DFO enhanced the tubularization and migration of HUVECs. We further confirmed in vivo the bone regeneration and tissue reconstruction stimulated by NG-TCS-DFO, using C57BL/6 mice. Our findings suggest that NG-TCS-DFO is a safe, robust and versatile platform for chronic periodontitis treatment.

Author Contributions

Guoxin Ma and Ke Xu contributed equally to this work. Leixiao Yu and Rainer Haag conceived the concept of this project. All the authors have contributed to writing this manuscript. The final version of this manuscript has been approved by all the authors.

Acknowledgements

Funded by the Deutsche Forschungsgemeinschaft (DFG, German Research Foundation) – Project ID 431232613 – SFB 1449, and – Project ID 434130070 – IRTG 2662. We thank the National Natural Science Foundation of China (82371014) and West China Hospital of Stomatology (QDJF2021-3) for financial support. The authors thank Dr. Mathias Dimde (Institut für Chemie und Biochemie, Freie Universität Berlin) for cryo-EM measurement. We thank Cathleen Hudziak for conducting the GPC measurement. The authors thank Salim Fazzani for HPLC analysis. We show great thanks to Dr. Rameez Ahmed for the AFM

measurement. We would also acknowledge Benjamin Allen (Boston, USA) for language polishing and proofreading. The Scheme. 1 is created on Biorender (http://Biorender.com). Open Access funding enabled and organized by Projekt DEAL.

Conflict of Interest

The authors declare no conflict of interest.

Data Availability Statement

The data that support the findings of this study are available in the supplementary material of this article.

Keywords: Periodontitis · Nanogel · Anti-bacteria · Anti-biofilm · Angiogenesis

[1] a) C. Berne, C. K. Ellison, A. Ducret, Y. V. Brun, *Nat. Rev. Microbiol.* **2018**, *16*, 616–627; b) G. Hajishengallis, T. Chavakis, J. D. Lambris, *Periodontol. 2000* **2020**, *84*, 14–34; c) D. F. Kinane, P. G. Stathopoulou, P. N. Papapanou, *Nat. Rev. Dis. Prim.* **2017**, *3*, 17038.

[2] a) I. Gotsman, C. Lotan, W. A. Soskolne, S. Rassovsky, T. Pugatsch, L. Lapidus, Y. Novikov, S. Masrawa, A. Stabholz, *J. Periodontol.* **2007**, *78*, 849–858; b) G. Hajishengallis, T. Chavakis, *Nat. Rev. Immunol.* **2021**, *21*, 426–440; c) G. Hajishengallis, *Nat. Rev. Immunol.* **2015**, *15*, 30–44.

[3] D. T. Graves, J. Li, D. L. Cochran, *J. Dent. Res.* **2010**, *90*, 143–153.

[4] a) W. Becker, L. Berg, B. E. Becker, *J. Periodontol.* **1979**, *50*, 234–244; b) F. Oliveira Costa, L. O. M. Cota, J. E. Costa, I. A. Pordeus, *J. Periodontol.* **2007**, *78*, 198–203; c) M. T. Pöllänen, J. I. Salonen, V.-J. Uitto, *Periodontol. 2000* **2003**, *31*, 12–31.

[5] a) D. L. Cochran, *J. Periodontol.* **2008**, *79*, 1569–1576; b) A. C. Tanner, *J. Oral Biosci.* **2015**, *57*, 18–26.

[6] a) D. Herrera, M. Sanz, S. Jepsen, I. Needleman, S. Roldán, *J. Clin. Periodontol.* **2002**, *29*, 136–159; b) D. Joshi, T. Garg, A. K. Goyal, G. Rath, *Drug Delivery* **2016**, *23*, 363–377.

[7] a) R. Wise, T. Hart, O. Cars, M. Streulens, R. Helmuth, P. Huovinen, M. Sprenger, *BMJ* **1998**, *317*, 609; b) M. Addy, M. V. Martin, *Oral Dis.* **2003**, *9*, 38–44; c) J. M. Goodson, *Periodontol. 2000* **1994**, *5*, 142–168.

[8] a) J. M. Goodson, S. Offenbacher, D. H. Farr, P. E. Hogan, *J. Periodontol.* **1985**, *56*, 265–272; b) H. Zazo, C. I. Colino, J. M. Lanao, *J. Controlled Release* **2016**, *224*, 86–102.

[9] K. S. Kornman, *J. Periodontol.* **1993**, *64*, 782–791.

[10] a) K. Forier, K. Raemdonck, S. C. De Smedt, J. Demeester, T. Coenye, K. Braeckmans, *J. Controlled Release* **2014**, *190*, 607–623; b) S. Xie, Y. Tao, Y. Pan, W. Qu, G. Cheng, L. Huang, D. Chen, X. Wang, Z. Liu, Z. Yuan, *J. Controlled Release* **2014**, *187*, 101–117.

[11] a) R. A. Jain, *Biomaterials* **2000**, *21*, 2475–2490; b) P. Bawa, V. Pillay, Y. E. Choonara, L. C. du Toit, *J. Biomed. Mater.* **2009**, *4*, 022001; c) S. Parveen, R. Misra, S. K. Sahoo, *Nanomedicine* **2012**, *8*, 147–166; d) E. Briones, C. Isabel Colino, J. M. Lanao, *J. Controlled Release* **2008**, *125*, 210–227.

[12] a) H. N. Bhargava, P. A. Leonard, *Am. J. Infect. Control.* **1996**, *24*, 209–218; b) B. A. Pancer, D. Kott, J. V. Sugai, F. S. Panagakos, T. M. Braun, R. P. Teles, W. V. Giannobile, J. S. Kinney, *J. Clin. Periodontol.* **2016**, *43*, 435–444.

[13] Y. Ikeda, K.-i. Hirano, N. Fukushima, Y. Sawa, *Eur. Heart J.* **2014**, *35*, 875–875.

[14] a) N. C. Andrews, *N. Engl. J. Med.* **1999**, *341*, 1986–1995; b) P. E. Hallaway, J. W. Eaton, S. S. Panter, B. E. Hedlund, *Proc. Natl. Acad. Sci. USA* **1989**, *86*, 10108–10112.

[15] a) J. Zhang, D. Tong, H. Song, R. Ruan, Y. Sun, Y. Lin, J. Wang, L. Hou, J. Dai, J. Ding, H. Yang, *Adv. Mater.* **2022**, *34*, 2202044; b) H. Xie, Z. Wang, R. Wang, Q. Chen, A. Yu, A. Lu, *Adv. Funct. Mater.* **2024**, *34*, 2401209; c) H. Chen, P. Jia, H. Kang, H. Zhang, Y. Liu, P. Yang, Y. Yan, G. Zuo, L. Guo, M. Jiang, J. Qi, Y. Liu, W. Cui, H. A. Santos, L. Deng, *Adv. Healthcare Mater.* **2016**, *5*, 907–918.

[16] a) P. Carmeliet, *Nat. Med.* **2000**, *6*, 389–395; b) R. A. D. Carano, E. H. Filvaroff, *Drug Discovery Today* **2003**, *8*, 980–989.

[17] L. Yu, Y. Hou, W. Xie, J. L. Cuellar-Camacho, Q. Wei, R. Haag, *Adv. Mater.* **2020**, *32*, 2006986.

[18] W. Chen, Y. Hou, Z. Tu, L. Gao, R. Haag, *J. Controlled Release* **2017**, *259*, 160–167.

[19] a) B. Liu, S. Thayumanavan, *J. Am. Chem. Soc.* **2017**, *139*, 2306–2317; b) S. Nowag, R. Haag, *Angew. Chem. Int. Ed.* **2014**, *53*, 49–51; c) S. Binauld, M. H. Stenzel, *Chem. Commun.* **2013**, *49*, 2082–2102.

[20] a) O. Wagner, B. N. S. Thota, B. Schade, F. Neumann, J. L. Cuellar, C. Böttcher, R. Haag, *Polym. Chem.* **2016**, *7*, 2222–2229; b) C. Nie, P. Pouyan, D. Lauster, J. Trimpert, Y. Kerkhoff, G. P. Szekeres, M. Wallert, S. Block, A. K. Sahoo, J. Dernedde, K. Pagel, B. B. Kaufer, R. R. Netz, M. Ballauff, R. Haag, *Angew. Chem. Int. Ed.* **2021**, *60*, 15870–15878.

[21] J. Mysak, S. Podzimek, P. Sommerova, Y. Lyuya-Mi, J. Bartova, T. Janatova, J. Prochazkova, J. Duskova, *J. Immunol. Res.* **2014**, *2014*, 476068.

[22] a) M. G. Escalada, J. L. Harwood, J. Y. Maillard, D. Ochs, *J. Antimicrob. Chemother.* **2005**, *55*, 879–882; b) I. Makarovsky, Y. Boguslavsky, M. Alesker, J. Lellouche, E. Banin, J.-P. Lellouche, *Adv. Funct. Mater.* **2011**, *21*, 4295–4304; c) D. Leaper, O. Assadian, N.-O. Hubner, A. McBain, T. Barbolt, S. Rothenburger, P. Wilson, *Int. Wound J.* **2011**, *8*, 556–566.

[23] P. E. Kolenbrander, R. J. Palmer, S. Periasamy, N. S. Jakubovics, *Nat. Rev. Microbiol.* **2010**, *8*, 471–480.

[24] a) Y. Li, R. A. Burne, *Microbiology* **2001**, *147*, 2841–2848; b) H. Koo, M. L. Falsetta, M. I. Klein, *J. Dent. Res.* **2013**, *92*, 1065–1073.

[25] a) C. Wan, S. R. Gilbert, Y. Wang, X. Cao, X. Shen, G. Ramaswamy, K. A. Jacobsen, Z. S. Alaql, A. W. Eberhardt, L. C. Gerstenfeld, T. A. Einhorn, L. Deng, T. L. Clemens, *Proc. Natl. Acad. Sci. USA* **2008**, *105*, 686–691; b) E. Chou, I. Suzuma, K. J. Way, D. Opland, A. C. Clermont, K. Naruse, K. Suzuma, N. L. Bowling, C. J. Vlahos, L. P. Aiello, G. L. King, *Circulation* **2002**, *105*, 373–379.

[26] M. E. Berman, Y. Xie, W. A. Muller, *J. Immunol.* **1996**, *156*, 1515–1524.

[27] J. E. Aubin, *Rev. Endocr. Metab. Disord.* **2001**, *2*, 81–94.

[28] T. Kishimoto, *Int. Immunol.* **2010**, *22*, 347–352.

Manuscript received: September 30, 2024
Accepted manuscript online: January 19, 2025
Version of record online: February 3, 2025